Synthesis of Rare Earth Doped Nano-Titanium Dioxide Grafted with Vinyl Functioned Siloxane Oligomer and the Properties of Its Electrorheological Fluid

Zhifeng Wang, Chunyan Xiao, Yuting Zhang, Defeng Wu, Kohji Yoshinaga, Ming Zhang

A silane coupling agent, 3-(methacryloxyl)propyl trimethoxysilane, was used for the *in-situ* surface modification of nano-titanium dioxide (TiO_2) and rare earth ion (Nd^{3+}) doped nano-TiO_2 (MPT – TiO_2, MPT – Nd – TiO_2) through sol-gel combined hydrothermal method to embed the particle surfaces with vinyl chain. Those surface modified particles were then further reacted with the vinyl functioned siloxane oligomer (VFSO) to obtain a novel electrorheological fluid (ERF). Fourier transform infrared (FT – IR), X-ray diffraction (XRD) and transmission electron microscopy (TEM) were used to characterize the structure of the surface modified particles. The rheological properties of the obtained ERF were also tested by rotational rheometer. It is found that both the MPT – TiO_2 and MPT – Nd – TiO_2 are nano-particles with anatase crystal structure. The ERF with grafted MPT – Nd – TiO_2 particles shows better anti-sedimentation stability and higher electrorheological responses than the ones with ungrafted particles has not grafted because the former can form stable three-dimensional network in the electric field. Moreover, the incorporation of rare earth ions (Nd^{3+}) can improves the polarization intensity of nano-particles, further enhancing electrorheological effect of the ERF.

Keywords: nano-titanium dioxide, rare earth, graft polymerization, vinyl functioned siloxane oligomer, electrorheological fluid.

Для получения электрореологической жидкости проводили модификацию поверхности нано-диоксидом титана (TiO_2) и редкоземельными ионами (Nd^{3+}) легированными нано-TiO_2 (MPT-TiO_2, MPT-Nd-TiO_2). Комбинированный гидротермический золь-гель метод со связующим силаном 3-(метакрилоксил)пропил триметоксисиланом применяли для встраивания частиц в виниловые цепочки. Затем на поверхности проходила реакция частиц с виниловым силоксановым олигомером, с формированием электрореологической жидкости. Для анализа структуры поверхности частиц использовали ИК-Фурье спектроскопию, рентгеноструктурный анализ и просвечивающую электронную микроскопию. Реологические свойства были также протестированы на вращательном реометре. Установлено, что обе структуры MPT-TiO_2 и MPT-Nd-TiO_2 представляют из себя нано-частицы с кристаллической структурой анатаза. Электрореологическая жидкость с частицами MPT-Nd-TiO_2 показывает лучшую антисе-диментационную стабильность и более высокие электрореологические свойства, чем у несвязанных частиц, так как первая может образовывать устойчивую трехмерную сетку в электрическом поле. Кроме того, включение редкоземельных ионов (Nd^{3+}) может повышать интенсивность поляризации нано-частиц и улучшать электрореологические свойства.

Ключевые слова: электрореологические жидкости, нано-диоксид титана, редкоземельные элементы, полимеризация.

Introduction

ERF is a kind of suspension system containing particles with high dielectric constant and low electrical conductivity that are dispersed in the liquid matrix of low dielectric constant. The microstructure of this kind suspension system will change in an electric field, and hence its physical properties will alter as a result. However, the poor stability of the anti-settlement of ERF highly restricts its industrial application [1 – 4] Thus, how to improve the stability of this suspension has attracted much interest. In recent years, the studies has focused on preparing nano-scaled solid particles, surface modification of solid particles and the polymer shell package, or adding surfactants in the suspension system [5 – 14]. Those work mainly concentrated on the solid particles, while ignoring the interaction between the solid particles and the liquid matrix. In other words, they isolate the two phases and have not combined them for integrative analysis. If this integrative analysis focuses on the controlled preparation of micro- or nano-structural composites, a range of meaningful phenomena would occur.

In this work, in order to obtain an ERF with higher anti-settlement stability, a silane coupling agent with vinyl chain, MPT, was used for *in-situ* surface modification of nano-titanium dioxide (TiO_2) and Nd^{3+} doped nano-TiO_2 (MPT – TiO_2 and MPT – Nd – TiO_2) to make the particle surface present reactivity. Then the surface modified particles were further reacted with the vinyl functioned siloxane oligomer to form a novel ERF. The microstructure, anti-settlement property and electrorheological effects were detailed characterized, aiming at establishing structure-properties of such novel ERF.

Experimental

Materials Preparation

Synthesis of Nd^{3+} doped nano-TiO_2 nano-particles

The Nd^{3+} doped nano-TiO_2 nano-particle (MPT – Nd – TiO_2) was prepared by sol-gel combined hydrothermal method. 0.01 mol neodymium oxide (Nd_2O_3, 99.999%) was reacted fully with superfluous hydrochloric acid (HCl, A.R.), followed by heating to distill out the excess HCl and the generated water. The generated neodymium chloride ($NdCl_3$) was dissolved with anhydrous alcohol (EtOH, A.R.) to form 0.1 mol·L^{-1} of the $NdCl_3$ – EtOH solution. Then, 0.01 mol tetrabutyl titanate (TBOT, A.R.), 0.001 mol MPT (silane coupling agent) and 0.01 mol acetic acid (HAc, A.R.) were mixed with 0.1 mol EtOH at room temperature and were stirred to get a uniform suspension (solution-A). At the same time, a certain amount of HCl was dropped into the mixture of 5 ml $NdCl_3$ – EtOH, 0.02 mol d-H_2O and EtOH in order to adjust the solution pH = 1 and then were stirred to get a uniform suspension (solution-B). Then, the solution-B was added into the solution-A slowly until a homogeneous and transparent sol was formed, in which the molar ratio of each substance TBOT: MPT: $NdCl_3$: EtOH: d-H_2O: HAc = 1: 0.1: 0.05: 20: 2: 1. The sol was then placed statically at 40°C to form a gel, followed by hydrothermal reaction at 200°C for 48 h. The product was washed by EtOH and acetone (Ac, A.R.) until the filtrate was neutral, and then was dried at room temperature in vacuum. Finally, the MPT *in-situ* modified nano-TiO_2 doped by Nd^{3+} particle was obtained and denoted as the MPT – Nd – TiO_2. At the same time, the above preparation process was also repeated but the $NdCl_3$ was not added, then the MPT – TiO_2 can be got.

Synthesis of ERF

2g MPT – TiO_2 or MPT-Nd-TiO_2 nano-particles were dispersed in 8 g vinyl silicone oil containing a certain amount of chloroform and were fully stirred with addition of the initiator benzoyl peroxide (BPO). The reactions were then maintained for 5h in N_2 atmosphere at 90 °C. The obtained system was distilled under vacuum to remove solvent and obtain a stable suspension, namely MPT – TiO_2 – *g*-VFSO or MPT – Nd – TiO_2 – *g*-VFSO electrorheological fluids. The suspension was further dried under vacuum at 65 °C before use.

2 g MPT – TiO_2 nano-particles were dispersed in 8 g vinyl silicone oil containing a certain amount of chloroform and were fully stirred. The obtained system was distilled under vacuum to remove solvent to obtain MPT – TiO_2/VFSO electrorheological fluids. The suspension was further dried in air at 100°C before use.

Characterization

The crystal structure of MPT – TiO_2 and MPT – Nd – TiO_2 particles were characterized by the XRD. The experiments were performed using a D8 advance diffractometer (BRUKER AXS Co., Germany) with Cu target and a rotating anode generator operated at 40 kV and 120 mA. The scanning rate was 2°/min from 20 to 75°.

The morphology of these two nano-particles were investigated by TEM (PHILIPS, Netherlands) with 120 kV accelerating voltage. 1 mg of the specimen was dispersed in 50 ml of EtOH followed by ultrasonic treating at 25°C for 15 min and then was dried onto carbon-coated copper grids before examination.

The reaction product of MPT – TiO_2 – *g*-VFSO was characterized using a TENSOR27 FTIR Spectroscopy (FTIR, BRUKER Co., Germany), and the VFSO and MPT – TiO_2 were also characterized for comparison. Thin film specimens were pressed with KBr power. All the FTIR spectra of specimen were obtained by coadding 64 scans and collected with the resolution of 2 cm^{-1}.

The sedimentation test: 10 ml MPT – TiO_2 – *g*-VFSO ERF containing 20 wt.% MPT – TiO_2 were placed in graduated flask. The values of horizontal scale for the phase interface were recorded every predetermined time during tests. The sedimentary ratio of ERF is calculated according to following relation [22, 23].

$$\text{Sedimentation ratio} = \frac{a}{10}, \qquad (1)$$

where a is sediment volume.

The electrorheological properties of the novel grafting electrorheological fluids of MPT – TiO_2 – *g*-VFSO and MPT – Nd – TiO_2 – *g*-VFSO compared with MPT – TiO_2/VFSO were then tested by a rotational rheometer (HAAKE RS600, Thermo Electron Co., U.S.A.) equipped with an electrical source with high level voltage. The samples about 1.0 mm in thickness were put in the parallel plate fixture at 25°C for 5 min, and then carry out the steady and dynamic shear measurements immediately. The steady shear sweep was first carried out to test the steady electrorheological measurements. The dynamic stress sweep was then carried out to determine a common linear region, stress of 0.2 Pa. Last, the small amplitude oscillatory shear (SAOS) was applied and the dynamic frequency sweep was carried out.

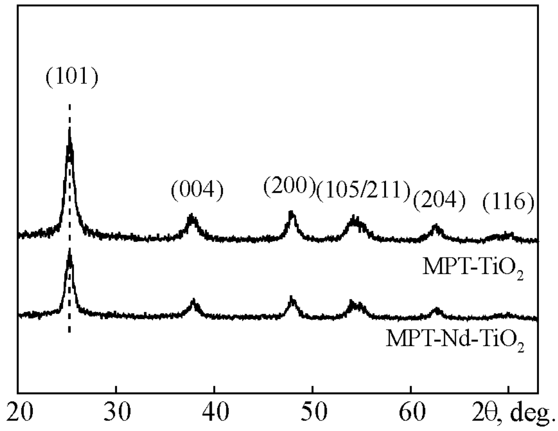

Fig. 1. XRD patterns of MPT – TiO_2 and MPT – Nd – TiO_2 nano-particles.

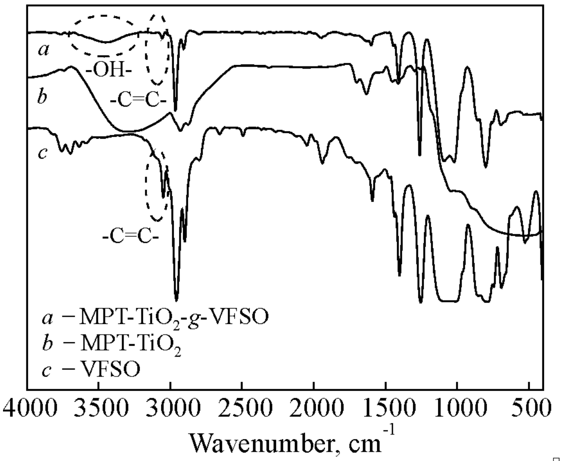

Fig. 2. FTIR spectrums of the MPT – TiO_2 – *g*-VFSO, MPT – TiO_2 and VFSO.

Results and discussion

Microstructure of nano-particles and their ERFs

The XRD patterns of MPT – TiO_2 and MPT – Nd – TiO_2 nano-particles are shown in fig. 1. Both of them show the characteristic pattern of TiO_2 with anatase phase [15 – 18]. Compared with that of the MPT – TiO_2, no evident differentiation can be observed on the MPT – Nd – TiO_2. However, the peaks become weaker and wider in the presence of Nd^{3+}. The crystal grain size can be obtained according to the Scherrer equation

$$D = \frac{K\lambda}{\beta\cos\theta}, \quad (2)$$

where K — dimensionless constant (0.89), 2θ — the diffraction angle, λ — the wavelength of the X-ray radiation (0.15406 nm) and β — the full width at half-maximum of the diffraction peak. The crystal grain size of MPT – TiO_2 nano-particle and MPT – Nd – TiO_2 nano-particle are 13.5 and 12.6 nm, respectively. This indicates that the rare earth ion (Nd^{3+}) substitute for Ti successfully and cause lattice distortion that prevents grain growth [19, 20].

Fig. 2 gives the FT-IR spectra for the MPT – TiO_2 – VFSO ERF, MPT and VFSO. It is clear that the – C = C – absorption band at about 3040 cm^{-1} still exists on MPT – TiO_2 – g-VFSO, but their intensity reduced remarkably. The –OH– stretching adsorption band at about 3500 cm^{-1} can also been observed on the MPT – TiO_2 – *g*-VFSO, which indicates that a certain degree of the graft copolymerization occurs between VFSO and MPT – TiO_2 by adding the initiator BPO [21].

Fig. 3 gives the TEM images for MPT – TiO_2 and MPT – Nd – TiO_2 nano-particles. Clearly, the MPT – TiO_2 spherical particles present good dispersion, showing uniform diameters of about 10 nm. After been doped by Nd^{3+}, the particles (MPT – Nd – TiO_2) keep their spherical shape while show reduced size in contrast to the MPT – TiO_2. This again confirms that Ti^{4+} ions have been doped into the TiO_2 particles modified by MPT successfully.

The anti-sedimentation properties of nano-ERFs

The anti-sedimentation property is vital to ERF because the electrorheological responses of an ERF system depend strongly on the sedimentation of the contained particles. Fig. 4 gives the time development of sedimentation ratios for the MPT – TiO_2 – *g*-VFSO and the MPT – TiO_2/VFSO systems. It is seen that the sedimentation nearly does not occur in the MPT – TiO_2 – *g*-VFSO suspension system even after 240 h. This is due to the good intersolubility between MPT – TiO_2 particles and continuous VFSO phase. The mesoscopic homogeneousness in that system prevents sedimentation of particles. Thus, the MPT – TiO_2 – *g*-VFSO suspension system shows far better stability than the MPT – TiO_2/VFSO suspension system.

The electrorheological property of nano-ERFs

The good anti-sedimentation property is only a premise to obtain good ERF, while the electrorheological response is the most important properties of an ERF. Fig. 5 gives steady electrorheological response for the MPT – TiO_2 – *g*-VFSO ERF at various levels of shear stress and voltage. It is seen that the system presents typical Newtonian flow behavior without electric field. Once in the electric field, the apparent viscosity (a) and the stress response (b) of the system increase with increasing electric field intensity evidently and, at the low level of shear rate, the system shows remarkable yield behavior, which is the characteristic of Bingham flow.

This evident electrorheological response is attributed to special morphology in the MPT – TiO_2 – *g*-VFSO ERF. As mentioned above, the graft reaction between VFSO chain and the surface –CH=CH– on the

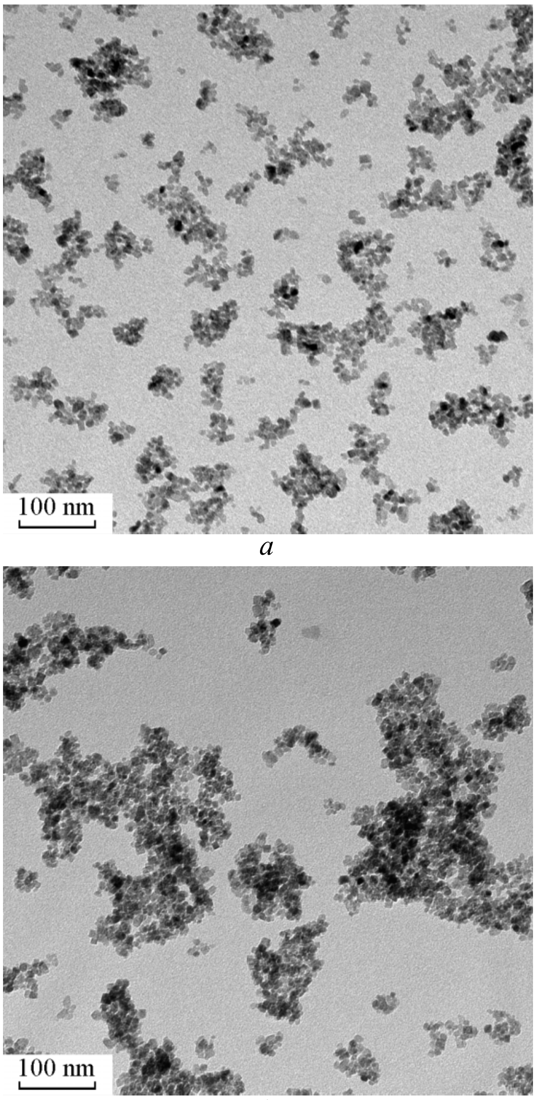

Fig. 3. TEM images for (a) MPT – TiO_2 and (b) MPT – Nd – TiO_2 nano-particles with a scale bar of 200 nm.

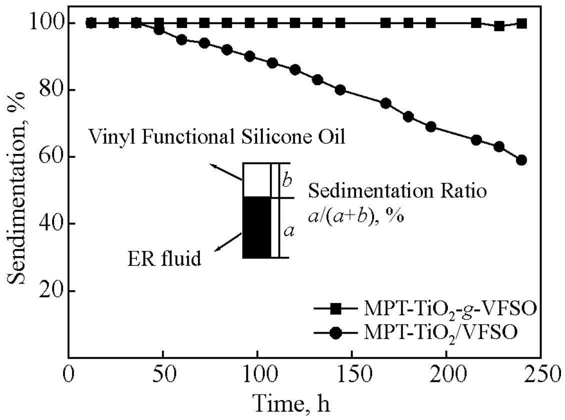

Fig. 4. Sedimentation ratios of the MPT – TiO_2 – *g*-VFSO and the MPT-TiO_2/VFSO *vs.* time.

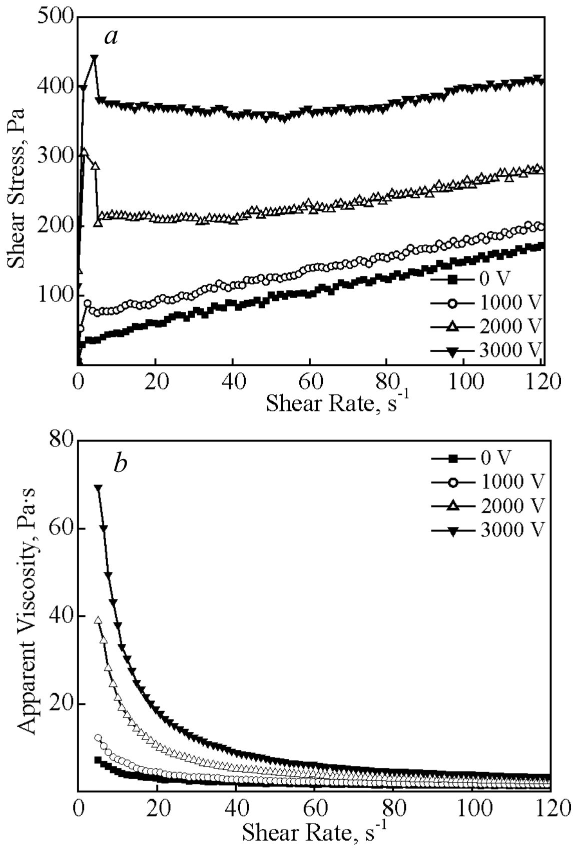

Fig. 5. The steady electrorheological properties of MPT – TiO_2 – *g*-VFSO ERF: *a* — shear stress, *b* — apparent viscosity *vs.* shear rate.

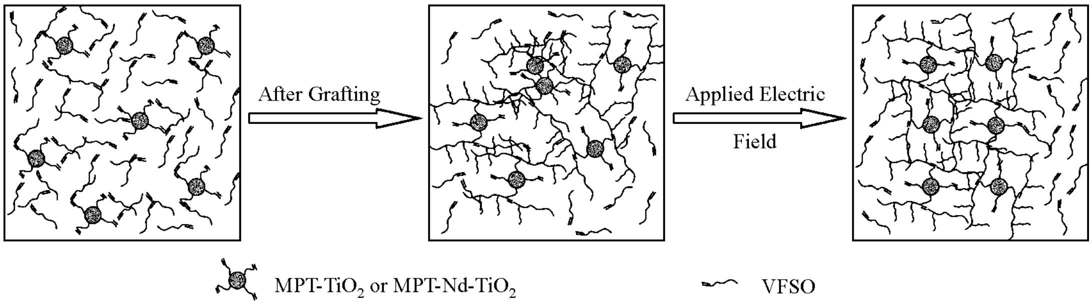

Fig. 6. Schematic diagrams of the micro-structural evolution for the ERF.

MPT – TiO_2 improves the intersolubility between particles and VFSO dispersive medium, finally leading to nice dispersion of particles. In addition, the VFSO chain on the surface of MPT – TiO_2 shows higher volume and longer length than that of MPT, which enhances the particle-particle interactions. In an electric field, those surface-modified particles are polarized, forming dipoles. The static force, as a result, makes them interacts among one another regularly. At lower level of electric field intensity (1,000 V), however, the static force is not strong enough to destroy the particle-particle interactions caused by the entanglement of those out-of-order surface VFSO chains. Thus, the system shows merely small increase of stress response and weak yield behavior. With increase of electric field intensity, the static force increases gradually and finally, promotes disentanglement of the surface VFSO chains and rearranges the particles, forming stable and regular three-dimensional network structure. In this case, the entanglement of the surface VFSO chains is not the counterwork impeding directional arrangement of particles, while becomes positive to maintain directional arrangement of particles in the shear flow. Accordingly, at lower level of electric field intensity (2,000 – 3,000 V), the system shows stronger stress response and yield behavior. This structural evolution is described schematically in fig. 6.

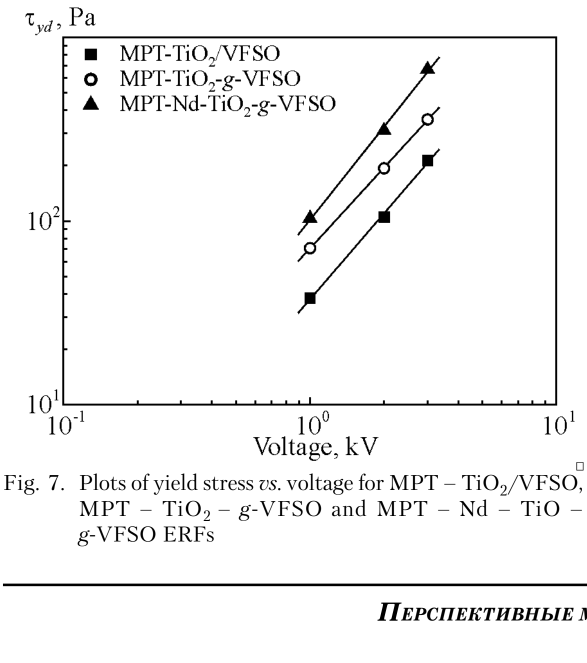

Fig. 7. Plots of yield stress *vs.* voltage for MPT – TiO_2/VFSO, MPT – TiO_2 – *g*-VFSO and MPT – Nd – TiO – *g*-VFSO ERFs

To further explore the effect of graft reaction and doped Nd^{3+} on the electrorheological properties of the ERF, it is necessary to study the electrorheological responses of various systems. Fig. 7 gives the electric field intensity dependence of yield stress for MPT – TiO_2 – *g*-VFSO, MPT – Nd – TiO_2 – *g*-VFSO and MPT – TiO_2/VFSO ERFs. Clearly, the yield stress (τ_y) for those three systems follows the relations of MPT – Nd – TiO_2 – *g*-VFSO > MPT – TiO_2 – *g*-VFSO > MPT – TiO_2/ VFSO, At 3,000 V, the τ_y value increases from 204.4 Pa (system without graft) to 359.2 Pa (grafted system), and further to 659.5 Pa (Nd^{3+} doped grafted system). This indicates that graft reaction and doped Nd^{3+} could enhance the electrorheological effect of the ERF. On the one hand, surface modification can improve the affinity between TiO_2 and VFSO, favoring the dispersion of particles and stabilization of network structure. On the other hand, the presence of Nd^{3+} could enhance polarization level of particles, further enhancing the electrorheological effect of the ERF [24].

In general, the yield stress (τ_y) and the electric field intensity (E_0) follow the relation [25 – 27]

$$\tau_y \propto AE_0^{\alpha}. \qquad (3)$$

Through linear fitting (fig. 7), the α values of 1.57, 1.46 and 1.68 are obtained for MPT – TiO_2/VFSO, MPT – TiO_2 – *g*-VFSO and MPT – Nd – TiO_2 – *g*-VFSO systems, respectively. The values range from 1 to 2, which is a characteristic value region for the suspension system [26], deviating more or less from classic polarization model ($\alpha = 2$) [28, 29]. For the system in this study, the particle concentration, shape and conductivity may all have influence on the a value [30], indicating that the polarization model might not used simply to describe the electrorheological effect of the ERF in this study.

It is well accepted that the dynamic rheology is a powerful tool to explore the mesoscopic structure of a

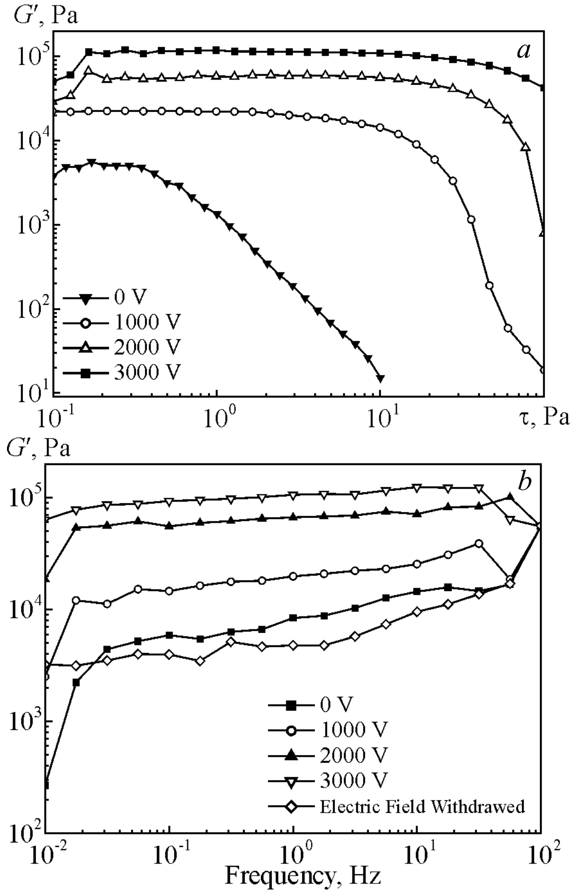

Fig. 8. The dynamic electrorheological properties of MPT – Nd – TiO_2 – *g*-VFSO ERF: *a* — storage modulus *vs.* shear stress, *b* — storage modulus *vs.* frequency.

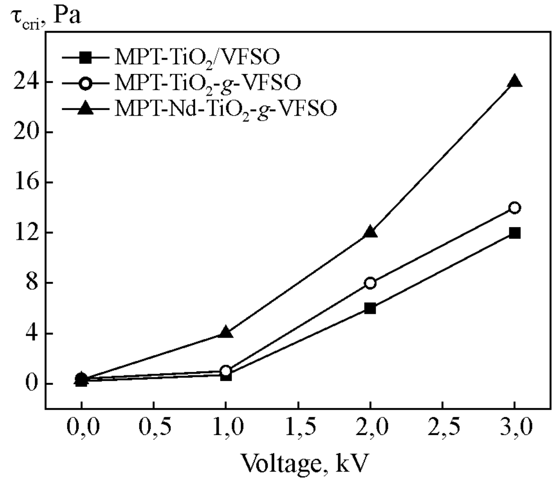

Fig. 9. Plots of the critical shear stress for shear thinning and storage modulus *vs.* voltage for MPT – TiO_2/VFSO, MPT – TiO_2 – *g*-VFSO and MPT – Nd – TiO_2 – *g*-VFSO ERFs.

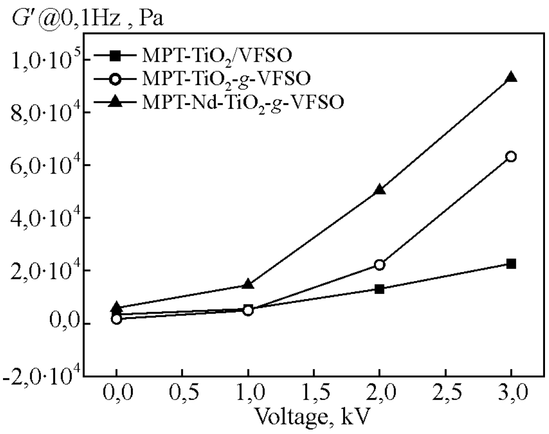

Fig. 10. Plots of storage modulus at 0.1 Hz *vs.* voltage for MPT – TiO_2/VFSO, MPT – TiO_2 – *g*-VFSO and MPT – Nd – TiO_2 – *g*-VFSO ERFs.

composite system [31 – 33]. To make further insight into the structural evolution of the ERF in the electric field, it is necessary to perform dynamic electrorheological tests on those ERFs. Fig. 8 gives the dynamic storage modulus (G') for the MPT – Nd – TiO_2 – *g*-VFSO ERF at various electric field intensity. It is seen that the system shows typical shear-thinning behavior at all levels of electric field intensity. However, G’ increases with increasing electric field intensity and, the linear viscoelastic region extends gradually (fig. 8*a*). This indicates that the particle-particle interactions increase in the electric field and, as a result, the formed network structure is more stable and needs more shear stress to be destroyed. It agrees with the discussion on fig. 6. As the stress is lower than 0.2 Pa, the system always shows Newtonian flow behavior. Hence the stress level of 0.1 Pa was determined to perform dynamic frequency sweep, as shown in fig. 8*b*. It is seen that G' of the MPT – Nd – TiO_2 – *g*-VFSO ERF is nearly non-dependent on frequency, showing typical solid-like behavior [34 – 37]. This also accords with the results from fig. 6. In addition, once the electric field is withdrawn, G' almost recoveries to the level of without electric field, indicating that the MPT – Nd – TiO_2 – *g*-VFSO ERF presents good reversible characteristic.

Fig. 9*a* gives the electric field intensity dependence of critical shear stress (τ_{cri}) as the ERF showing shear thinning behavior. It is seen that τ_{cri} values increase with increase of electric field intensity for all ERF systems. At identical levels of electric field intensity, τ_{cri} values for the three ERF systems in this work show the order of MPT – Nd – TiO_2 – *g*-VFSO > MPT – TiO_2 – *g*-VFSO > MPT – TiO_2/VFSO, which agrees with the relations of τ_y among those three ERF systems.

Generally, the low-frequency viscoelasticity is corresponding to the long-term structure relaxation of a composite system. Fig. 10 gives low-frequency modulus (at 0.1 Hz) as a function of electric field intensity for all three ERFs. As expected, it is clear that the MPT – Nd – TiO_2 – *g*-VFSO system shows far higher *G*' than those of the other two systems especially at higher electric field intensity. The *G*' values increase from 22730 Pa of the MPT – TiO_2/VFSO system to 93190 Pa of the MPT – Nd – TiO_2 – *g*-VFSO system by about 3.1 times. This again confirms that the doped Nd^{3+} enhances polarization levels of particles in the ERF.

Conclusions

In this work, the MPT – TiO_2 and MPT – Nd – TiO_2 nano-particles with anatase crystal structure were synthesized through sol-gel combined hydrothermal method. The VFSO was then further grafted onto those particles to obtain the novel grafting ERF with excellent anti-sedimentation stability. The grafted particles can form stable and ordered three-dimensional network structure in the electric field. The doped Nd^{3+} can further enhance polarization levels of particles. Both contribute to excellent electrorheological effects of the obtained ERF.

This work was supported by the research grants from the National Natural Science Foundation of China (No.50873058) and the Key Program of Jiangsu Province (No.06KJA15011).

References

1. Espin M.J., Delgado A.V., Gonz′alez-Caballero F., Rejon L. Rheological Properties of a Model Colloidal Suspension under Large Electric Fields of Different Waveforms. Journal of Non-Newtonian Fluid Mechanics, 2007, v. 146, February, p. 125 – 135.
2. Tse K.L., Shine A.D. Steady-state Electrorheology of Nematic Poly(*n*-hexyl isocyanate) Solutions. Macromolecules, 2000, v. 33, April, p. 3134 – 3141.
3. Ko Y.G., Sung B.H., Choi U.S. Electrorheological Properties of Aminated Chitosans. Colloids and Surfaces A: Physicochemical and Engineering Aspects, 2007, v. 305, September, p. 120 – 125.
4. Ha J., Yang S. Rheological Responses of Oi1-in Oil Emulsions in an Electric Field. Journal of Rheology, 2000, v. 44, March, p. 235 – 256.
5. Belza T., Pavlinek V., Saha P., Quadrat O. Electrorheological Properties of Suspensions of Silica Nanoparticles Modified by Urea and *N,N*-dimethylformamide. Colloids and Surfaces A: Physicochemical and Engineering Aspects, 2007, v. 297, April, p. 142 – 146.
6. Wen W.J., Huang X., Yang S., Lu K., Sheng P. Particle Size Scaling of the Giant Electrorheological Effect. Applied Physics Letters, 2004, v. 85, July, p. 299 – 301.
7. Cheng Q.L., Pavlinek V., He Y., Lengalova A., Li C.Z., Saha P. Structural and Electrorheological Properties of Mesoporous Silica Modified with Triethanolamine. Colloids and Surfaces A: Physicochemical and Engineering Aspects, 2008, v. 318, April, p. 169 – 174.
8. Cao J.G., Shen M., Zhou L.W. Preparation and Electrorheological Properties of Triethanolamine Modified TiO_2. Journal of Solid State Chemistry, 2006, v. 179, May, p. 1565 – 1568.
9. Chuan W., Zhu Y.H., Yang X.L., Li C.Z. One-pot Synthesis of Polyaniline Doped in Mesoporous TiO_2 and Its Electrorheological Behavior. Material Science and Engineering B, 2007, v. 137, February, p. 213 – 216.
10. Choi C.S., Park S.J., Choi H.J. Carbon Nanotube/ Polyaniline Nanocomposites and Their Electrorheological Characteristics under an Applied Electric Field. Current Applied Physics, 2007, v. 7, May, p. 352 – 355.
11. Yilmaz H., Degirmenci M., Unal H.I. Electrorheological Properties of PMMA–b–PSt Copolymer Suspensions. Journal of Colloid and Interface Science, 2006, v. 293, January, p. 489 – 495.
12. Di K., Zhu Y., Yang X., Li C. Electrorheological Behavior of Urea-doped Mesoporous TiO_2 Suspensions. Colloids and Surfaces A: Physicochemical and Engineering Aspects, 2006, v. 280, June, p. 71 – 75.
13. Wang B., Zhao X. Core/shell Nanocomposite Based on the Local Polarization and Its Electrorheological Behavior. Langmuir, 2005, v. 21, July, p. 6553 – 6559.
14. Wei C., Zhu Y., Jin Y., Yang X., Li C. Fabrication and Characterization of Mesoporous TiO_2/Polypyrrole-based Nanocomposite for Electrorheological Fluid. Materials Research Bulletin, 2008, v. 43, December, p. 3263 – 3269.
15. Wang Z.Y., Xia D.G., Chen G., Yang T., Chen Y. The Effects of Different Acids on the Preparation of TiO_2 Nanostructure in Liquid Media at Low Temperature. Materials Chemistry and Physics, 2008, v. 111, October, p. 313 – 316.
16. Chen X.B., Mao S.S. Titanium Dioxide Nanomaterials: Synthesis, Properties, Modifications, and Applications. Chemical Reviews, 2007, v. 107, July, p. 2891 – 2959.
17. Biju K.P., Jain M.K. Effect of Crystallization on Humidity Sensing Properties of Sol–gel Derived Nanocrystalline TiO_2 Thin Films. Thin Solid Films, 2008, v. 516, February, p. 2175 – 2180.
18. Yue L., Zhang X.M. Preparation of Highly Dispersed CeO_2/TiO_2 Core-shell Nanoparticles. Materials Letters, 2008, v. 62, August, p. 3764 – 3766.
19. Sekiyama, Suga S., Fujikawa M., Imada S. Electronic States of Charge Ordering $Nd_{0.5}Sr_{0.5}MnO_3$ Probed by Photoemission. Physical Review B, 1999, v. 59, June, p. 15528 – 15532.
20. Tonejc A.M., Djerdj I., Tonejc A. Evidence from HRTEM Image Processing, XRD and EDS on Nanocrystalline Iron-doped Titanium Oxide Powders. Material Science and Engineering B, 2001, v. 85, August, p. 55 – 63.
21. Dai S.J., Yang C.S., Qiu G.M., Zhang M., Pan S.L. Research on Electrorheological Fluid Containing Rare Earth Cerium. Journal of Rare Earths, 2007, v. 25, December, p. 49 – 53.

22. Wang B.X., Zhao X.P., Zhao Y., Ding C.L. Titanium Oxide Nanoparticle Modified with Chromium Ion and Its Giant Electrorheological Activity. Composites Science and Technology, 2007, v. 67, November, p. 3031 – 3038.
23. Lee H.J., Chin B.D., Yang S.M., Park O.O. Surfactant Effect on the Stability and Electrorheological Properties of Polyaniline Particle Suspension. Journal of Colloid and Interface Science, 1998, v. 206, October, p. 424 – 438.
24. Zhao X.P., Yin J.B. Preparation and Electrorheological Characteristics of Rare-earth-doped TiO_2 Suspensions. Chemistry of Materials, 2002, v. 14, May, p. 2258 – 2263.
25. Yin J.B., Zhao X.P. Preparation and Electrorheological Activity of Mesoporous Rare-Earth-Doped TiO_2. Chemistry of Materials, 2002, v. 14, November, p. 4633 – 4640.
26. Sung J.H., Jang W.H., Choi H.J., Jhon M.S. Universal Yield Stress Function for Biocompatible Chitosan Based-electrorheological Fluid: Effect of Particle Concentration. Polymer, 2005, v. 46, December, p. 12359 – 12365.
27. Yin J.B., Zhao X.P., Xia X., Xiang L.Q., Qiao Y.P. Electrorheological Fluids Based on Nano-fibrous Polyaniline. Polymer, 2008, v. 49, p. September, p. 4413 – 4419.
28. Klingenberg D.J., Van S.F., Zukoski C.F. The Small Shear Rate Response of Electrorheological Suspensions. I. Simulation in the Point–dipole Limit. Journal of Chemical Physics, 1991, v. 94, May, p. 6160 – 6169.
39. Tsuda K., Takeda Y., Ogura H., Otsubo Y. Electrorheological Behavior of Whisker Suspensions under Oscillatory Shear. Colloids and Surfaces A: Physicochemical and Engineering Aspects, 2007, v. 299, May, p. 262 – 267.
30. Kim S.G., Lim J.Y., Sung J.H., Choi H.J., Seo Y. Emulsion Polymerized Polyaniline Synthesized with Dodecylbenzene-sulfonic Acid and Its Electrorheological Characteristics: Temperature Effect. Polymer, 2007, v. 48, October, p. 6622 – 6631.
31. Wu D.F., Zhang Y.S., Zhang M., Yu W. Selective Localization of Multiwalled Carbon Nanotubes in Poly (ε-caprolactone)/Polylactide Blend. Biomacromolecules, 2009, v. 10, February, p. 417 – 424.
32. Wu D.F., Wu L.F., Zhang M., Zhou W.D., Zhang Y.S. Morphology Evolution of Nanocomposites Based on Poly(phenylene sulfide)/Poly(butylene terephthalate) Blend. Journal of Polymer Science: Part B: Polymer Physics, 2008, v. 46, June, p. 1265 – 1279.
33. Wu D.F., Zhang Y.S., Zhang M., Zhou W.D. Phase Behavior and Its Viscoelastic Response of Polylactide/Poly(ε-caprolactone) blend. European Polymer Journal, 2008, v. 44, July, p. 2171 – 2183.
34. Wu D.F., Sun Y.R., Wu L., Zhang M. Linear Viscoelastic Properties and Crystallization Behavior of Multi-Walled Carbon Nanotube/Polypropylene Composites. Journal of Applied Polymer Science, 2008, v. 108, May, p. 1506 – 1513.
35. Wu D.F., Wu L., Zhang M. Rheology of Multi-Walled Carbon Nanotube/Poly(butylenes terephthalate) Composites. Journal of Polymer Science: Part B: Polymer Physics, 2007, v. 45, August, p. 2239 – 2251.
36. Wu D.F., Wu L., Sun Y.R., Zhang M. Rheological Properties and Crystallization Behavior of Multi-Walled Carbon Nanotube/Poly(ε-caprolactone) Composites. Journal of Polymer Science: Part B: Polymer Physics, 2007, v. 45, December, p. 3137 – 3147.
37. Wu D.F., Wu L., Wu L.F., Zhang M. Rheology and Thermal Stability of Polylactide/Clay Nanocomposites. Polymer Degradation and Stability, 2006, v. 91, December, p. 3149 – 3155.

Zhifeng Wang — *School of Chemistry and Chemical Engineering, Yangzhou University (Jiangsu, PR China), Provincial Key Laboratory of Environmental Material and Engineering (Jiangsu, PR China).*

Chunyan Xiao — *School of Chemistry and Chemical Engineering, Yangzhou University (Jiangsu, PR China), Provincial Key Laboratory of Environmental Material and Engineering (Jiangsu, PR China).*

Yuting Zhang — *School of Chemistry and Chemical Engineering, Yangzhou University (Jiangsu, PR China), Provincial Key Laboratory of Environmental Material and Engineering (Jiangsu, PR China).*

Defeng Wu — *School of Chemistry and Chemical Engineering, Yangzhou University (Jiangsu, PR China), Provincial Key Laboratory of Environmental Material and Engineering (Jiangsu, PR China).*

Kohji Yoshinaga — *Department of Applied Chemistry, Faculty of Engineering, Kyushu Institute of Technology (Tobata, Kitakyushu, Japan).*

Ming Zhang — *School of Chemistry and Chemical Engineering, Yangzhou University (Jiangsu, PR China), Provincial Key Laboratory of Environmental Material and Engineering (Jiangsu, PR China), E-mail: lxyzhangm@yzu.edu.cn.*